PLOS ONE

Analysis of Multiple B-Value Diffusion-Weighted Imaging in Pediatric Acute Encephalopathy

Yasuhiko Tachibana[1,2,3], Noriko Aida[2,3], Tetsu Niwa[3,4], Kumiko Nozawa[3], Kouki Kusagiri[3], Kana Mori[3], Kazuo Endo[3], Takayuki Obata[1,2]*, Tomio Inoue[2]

1 Research Center for Charged Particle Therapy, National Institute of Radiological Sciences, Inage-ku, Chiba, Japan, 2 Department of Radiology, Yokohama City University Graduate School of Medicine, Kanazawa-ku, Yokohama, Japan, 3 Department of Radiology, Kanagawa Children's Medical Center, Minami-ku, Yokohama, Japan, 4 Department of Radiology, Tokai University School of Medicine, Isehara, Japan

Abstract

Acute encephalopathy is a disease group more commonly seen in children. It is often severe and has neurological sequelae. Imaging is important for early diagnosis and prompt treatment to ameliorate an unfavorable outcome, but insufficient sensitivity/specificity is a problem. To overcome this, a new value (fraction of high b-pair (F_H)) that could be processed from clinically acceptable MR diffusion-weighted imaging (DWI) with three different b-values was designed on the basis of a two-compartment model of water diffusion signal attenuation. The purpose of this study is to compare F_H with the apparent diffusion coefficient (ADC) regarding the detectability of pediatric acute encephalopathy. We retrospectively compared the clinical DWI of 15 children (1–10 years old, mean 2.34, 8 boys, 7 girls) of acute encephalopathy with another 16 children (1–11 years old, mean 4.89, 9 boys, 7 girls) as control. A comparison was first made visually by mapping F_H on the brain images, and then a second comparison was made on the basis of 10 regions of interest (ROIs) set on cortical and subcortical areas of each child. F_H map visually revealed diffusely elevated F_H in cortical and subcortical areas of the patients with acute encephalopathy; the changes seemed more diffuse in F_H compared to DWI. The comparison based on ROI revealed elevated mean F_H in the cortical and subcortical areas of the acute encephalopathy patients compared to control with significant difference (P<0.05). Similar findings were observed even in regions where the findings of DWI were slight. The reduction of mean ADC was significant in regions with severe findings in DWI, but it was not constant in the areas with slighter DWI findings. The detectability of slight changes of cortical and subcortical lesions in acute encephalopathy may be superior in F_H compared to ADC.

Introduction

Acute encephalopathy is a generic term for brain dysfunction of acute onset that often occurs subsequent to infectious diseases with fever, such as influenza and human herpes virus type 6 [1,2]. It is most common in infants and young children, is manifested clinically with stupor/coma and febrile seizure, and is often severe and prolonged [3]. Magnetic resonance imaging (MRI), especially high signal intensity in diffusion-weighted images (DWI), is known to be useful for detecting brain lesions [4–10]. Recently, several subtypes of acute encephalopathy have been categorized on the basis of MRI findings and clinical manifestations: acute necrotizing encephalopathy (ANE) [11,12], hemorrhagic shock and encephalopathy syndrome (HSES) [2], clinically mild encephalitis/encephalopathy with reversible splenial lesion (MERS) [10], and acute encephalopathy with biphasic seizures and late reduced diffusion (AESD) [6,8,10]. The characteristic findings, outcome, recommended treatment and genetic background for each subtype are gradually becoming clear [2,7,9,10,12–17], but the pathological mechanisms are still uncertain, and many cases of acute encephalopathy are unspecific and could not be directly categorized into the above subtypes [1,3,7,15].

The outcome of acute encephalopathy, except MERS, is often unfavorable [1,2,7,9,12]. Neurologic sequelae and even death are quite common. Diagnosis and treatment (e.g. steroid, human immunoglobulin and hyperthermia [2,10]) in the early stage are assumed to be crucial for ameliorating brain damage [5,9]. In this respect, rapid diagnosis by MRI is very important, but the findings, as aforementioned, are often unspecific, and they change remarkably with the time course even in typical cases. For example, reduced subcortical water diffusion is mentioned as an important hallmark of AESD, but it is also found in various brain lesions including other categories of (or uncategorizable) encephalopathies [5]. In addition, this finding in AESD is found best at 3–9 days from onset, but usually not in the earlier days or the later days (mild reduced diffusion in cortex may be found instead) [6,8,10]. For these reasons, both sensitivity and specificity of the DWI findings are not sufficient at present.

The reduced diffusion of acute encephalopathy was previously discussed on the basis of visual assessments of DWI, which is intrinsically related to the apparent diffusion coefficient (ADC) calculated by the following monoexponential equation using two different b-values:

$$S_b / S_0 = \exp(-bD) \qquad (1)$$

where S_b and S_0 indicate the signals with and without diffusion sensitizing gradients, b indicates the b-value, and D indicates ADC. However, the calculated values are sometimes misleading when applying different b-values in DWI because the signal attenuation does not always follow Eq. 1 in vivo. To compensate for this limitation, another model of signal attenuation that considers two separate diffusion components (fast and slow components) with exchange has been well discussed [18–27]. This two-compartment model is given by this biexponential equation:

$$S_b / S_0 = (1-f_s) * \exp(-bD_f) + f_s * \exp(-bD_s) \quad (2)$$

where fs indicates the fraction of the slow diffusion component, and Df and Ds indicate ADC of each fast and slow diffusion component, respectively. This equation (Eq. 2) is known to fit the experimental signal attenuation better than Eq. 1, and thus is often adopted for discussing in vivo water diffusion.

The detailed construction of the two compartments and their kinetics (balance, exchange) are not well established, but the parameters D_f, D_s, and f_s have been discussed previously to characterize tissue properties in a pathologic context of the human brain, such as ischemia, edema, tumor, and post-radiation [18,20,21,28]. Application of this model to the prostate [23] and mammalian glands [24,25] was also reported. However, it is not easy to calculate the exact fraction (f_s) in clinics because it requires a relatively large amount of data acquired from many different b-values (= longer scan time), a circumstance particularly unsuitable for acute encephalopathy patients, as it is risky, because of the disease severity, to stay in the MRI apparatus for an extended period. In addition, longer scan time directly increases the risk of failing the scan, as the duration of needing to remain still is also necessarily prolonged. This general problem in children can usually be managed by sedation agents, but seizures that can occur in acute encephalopathy might require extra doses, which also pose a risk for the severe state.

In this study, we designed a more simplified value "fraction of high b-pair (F_H)" related to the fraction of the two compartments. The purpose of this study is to compare F_H with ADC in terms of the detectability of pediatric acute encephalopathy, and to discuss its significance.

Materials and Methods

Ethics Statement

This retrospective study was approved by the ethics committee of the Kanagawa Children's Medical Center, where all of the clinical data in this study was acquired. Written informed consent was waived by the ethics committee.

Subjects

We searched our brain MRI database for pediatric patients (under 12 years old) who had undergone the four b-value diffusion-weighted imaging sequence (4bDWI, described later) as part of their clinical examination, and then designed two clinical groups for comparison: control group and encephalopathy group. The control group included patients who had undergone MRI examination for their neurologic symptoms but no abnormal imaging findings including 4bDWI had been found, and also whose symptoms were transient and disappeared without sequelae.

The encephalopathy group included patients who had ultimately been diagnosed with acute encephalopathy based on their clinical findings in addition to the abnormal DWI high intensity area found in their cerebrum. The clinical findings included continued consciousness insufficiency for at least 24 hours except sedation for hypothermia and/or intubation. Only patients with unfavorable outcome (death, or remaining neurologic sequelae such as impaired consciousness, spasticity) were included in the encephalopathy group (thus, patients with MERS were not included), and if MRI had been performed within 7 days from onset. For patients diagnosed as AESD, a secondary seizure was considered as the onset for this criterion.

For both groups, patients less than one year old were excluded to avoid the heterogeneity of myelin development, which it may affect water diffusion. Patients with metabolic diseases, prominent cerebral dimorphisms (e.g. corticogyral malformation, diffuse volume loss of brain from some other previous disease, chronic infarction), and severe motion affection on 4bDWI were excluded from both groups. Finally, 16 (1–11 years old, mean 4.89, 9 boys, 7 girls) and 15 patients (1–10 years old, mean 2.34, 8 boys, 7 girls) were selected for the control and encephalopathy groups, respectively. Indications for MRI examination of the control group were convulsion with a fever over 38°C (n = 4), convulsion (n = 2), suspicion of slight cognitive or motor impairment (n = 5), and other unspecific symptoms (n = 5). Definite diagnoses of the encephalopathy group were AESD (n = 5), ANE (n = 1), and other nonspecific encephalopathies (n = 9).

MR Imaging

All MR imaging was performed using a 3T MRI system (Verio 3T; SIEMENS, Germany) with either a 12-channel head coil or a combination of two 4-channel flex coils, depending on head size and age. Patients younger than 6 years and/or uncooperative regarding staying still were sedated during the imaging. Routine clinical MR imaging sequences in our institution consisted of transverse and sagittal T1-weighted spin-echo imaging, and transverse and coronal T2-weighted fast spin-echo imaging. Additional planes and sequences, such as fluid-attenuated inversion recovery imaging, diffusion-weighted imaging (b-value at 1000 sec/mm^2), susceptibility-weighted imaging, contrast enhanced T1-weighted spin-echo imaging, and magnetic resonance spectroscopy were obtained depending on the disease and the patient's condition. 4bDWI was also performed as an additional sequence when the patient was believed to have abnormalities that might not have been assessed sufficiently by the normal routine DWI sequence, but only if the clinical situation was stable and the benefit of the examination was believed to exceed the risk of the longer scanning time. This point was decided by an experienced board-certified pediatric neuroradiologist (N.A., 27-year experience) assisted by a board-certified pediatric neurologist attending the MRI system during the entire examination.

Four b-value diffusion-weighted imaging sequence (4bDWI). The outline parameters of the DWI sequence assessed in this study are shown in Table 1. All images were obtained in axial slices using the spin-echo-type single-shot echo planner imaging (EPI) technique. A parallel imaging technique for a multi-channel detector (GRAPPA: Generalized Autocalibrating Partially Parallel Acquisition) was applied. Motion probing gradients (MPG) were applied by Twin-Refocus-Spin-Echo technique. They were set in 3 orthogonal directions (anterior-posterior, left-right, cranio-caudal) separately, making three different image series. Trace DWI images, were then generated as their geographic mean. Imaging was automatically repeated four times to acquire four DWI image series with different b-values (the b-value was

Table 1. Outline of 4bDWI sequence.

MRI	3T MAGNETOM Verio, SIEMENS
Coil	12 ch head coil/4 ch flex coil
b-value	0, 500, 1500, 2500
TR/TE (msec)	7500/125
NEX	2
Matrix	Base 128 (Phase 70%)
FOV (mm)	200
Slice thickness (mm)	3
Band width (Hz/pixel)	1184
Scan time	2 min 54 sec

4bDWI: Four b-value diffusion-weighted imaging sequence, TR: repetition time, TE: echo time, NEX: number of excitations, FOV: field of view.
doi:10.1371/journal.pone.0063869.t001

converted in every repetition, i.e., b = 0, 500, 1500, 2500 sec/mm^2). Hence, four trace DWI image series with different b-values, respectively, were finally obtained.

Confirmation of Signal to Noise Ratio (SNR)

To confirm that there were enough SNR even in DWI images acquired at b = 2500 as described above, the following assessments were done in each patient of both groups. First, ROI was manually set at the center of the head of right or caudate nucleus; the b = 0 image was used. This procedure was performed by a board-certified radiologist. Then the ROI was automatically copied and also applied to the b = 2500 image. Finally, the mean signal intensity of the pixels included in the ROI at b = 2500 was divided by the standard deviation of their signal intensity at b = 0. The SNR was considered sufficient when this ratio was >3.0. The difference between the two groups was also assessed statistically using the Mann-Whitney test. A P-value <0.05 was considered significant.

Calculation of F_H

F_H was calculated from the signal intensities of b = 500, 1500, 2500 (S_{500}, S_{1500}, S_{2500}). First, two different theoretical signal intensities of b = 0 (S_{0low} and S_{0high}) were calculated from the signal intensity of the lower b-value pair (S_{500}, S_{1500}) and the higher b-value pair (S_{1500}, S_{2500}), respectively, based on the assumption of monoexponential signal attenuation (Introduction, Eq. 1). The former equals the y-intercept of the line connecting S_{500} and S_{1500} on a semi-logarithmic graph (b-value as x-axis, and logarithm of signal intensity as y-axis), while the latter equals the y-intercept of the line connecting S_{1500} and S_{2500} on the same graph. Then, F_H was calculated by S_{0high}/S_{0low} (Fig. 1).

F_H Mapping

F_H was calculated pixel-by-pixel for each of the obtained 4bDWI data. Then, F_H was mapped on the original image data so that it could be evaluated just like the usual MR images in clinics.

We applied several masking steps to each slice of the F_H map to exclude background (air) pixels and cerebrospinal fluid (CSF) pixels. First, to exclude background pixels, we excluded pixels whose signal intensities of b-values = 0, 500, 1500, 2500 did not decline in this order. Pixels from noise might be excluded by approximately 96% (1 − 1/(4!)) by this procedure, because their signal intensity should be in random order. Second, to exclude CSF pixels, we excluded the pixels from which the ADC
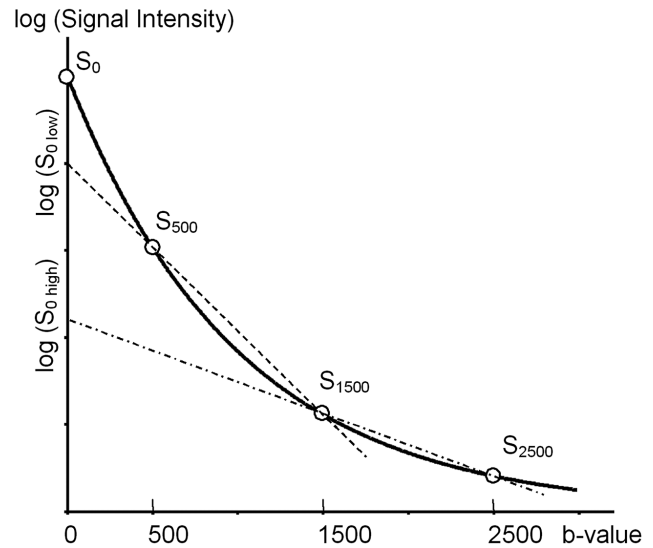

Figure 1. Calculation of F_H. The graph illustrates typical in vivo signal attenuation of diffusion-weighted imaging (DWI). S_0 to S_{2500} are the signal intensities of the corresponding b-values. S_{0high} and S_{0low} are the theoretical S_0 values calculated from a different data pair (pair of S_{500} and S_{1500}, and pair of S_{1500} and S_{2500}, respectively) using a monoexponential fitting (which becomes a straight line in this semi-logarithmic graph). Fraction of high b-pair (F_H) equals S_{0high}/S_{0low}.
doi:10.1371/journal.pone.0063869.g001

calculated from the signal intensities of b = 0 and 1500 (monoexponential fitting (Introduction, Eq. 1)) was over 1.5×10^{-3} mm^2/sec. Finally, binary neighborhood operations were applied to exclude the remaining background/noise pixels around the pixels of brain parenchyma; "erosion" and "dilation", both based on the 4-connected neighborhood, were performed in this order. After these operations, smoothing of the remaining image (consisting mostly of the pixels of brain parenchyma) was done by mean filtering: each pixel value was replaced by the mean value of its 8-connected neighborhoods and itself (9 pixels in total). The pixels masked by the previous masking procedure were excluded if they were included in these 9 pixels. These mapping operations as well as the other operations in this study on the acquired DWI images were all performed using our in-house software developed with a commercial analysis package (Matlab version R2007b, MathWorks Inc., Natick, MA, USA).

ROI-based Study

ROI setting on DWI images. In each patient, two specific slices were first selected for evaluation: one slice at the level of the cerebral hemisphere, the most cranial slice in which both lateral ventricles are demonstrated, and the other at the level of cerebral basal ganglia, in which both the genu and the splenium of the corpus callosum are most broadly demonstrated. Second, the resolution of each image was increased to four times higher. Third, 10 ROIs in total were set on the slices (Fig. 2, A,B). Detailed criteria were as follows. All ROIs included only the cerebral cortex and subcortical white matter as completely as possible; ROIs 1 to 4 were set on the slice of the cerebral hemisphere; ROI 1: frontal lobe of left cerebral hemisphere, excluding internal cerebral cortex/subcortical white matter; ROI 2: temporal lobe of left cerebral hemisphere, excluding internal cerebral cortex/subcortical white matter; ROIs 3, 4: conformed to criteria of ROIs 1, 2 at right cerebral hemisphere; ROIs 5 to 10 were set on the slice of cerebral basal ganglia; first, the left cerebral hemisphere, excluding

internal cerebral cortex/subcortical white matter, was selected; then the area was equally radially separated into three areas, according to the length along the brain surface; these regions corresponded to ROIs 5, 6, 7 in this order from rostral to dorsal; ROIs 8, 9, and 10: conformed to the criteria of ROIs 6, 7, 8 at the right cerebral hemisphere. To have the ROIs include only cortex and subcortical white matter as completely as possible, they were first manually set on DWI images (b = 1500) while being careful to include deep white matter as little as possible. Then, to exclude CSF pixels, the pixels from which the ADC (calculated from DWI images of b = 0 and 1500) was higher than 1.50×10^{-3} mm/sec^2, were excluded automatically from the manually designed ROIs (Fig. 2, C,D). These ROIs designed on DWI images of b = 1500 were copied and also applied to DWI images of b = 0, 500, and 2500 automatically.

The averaged signal intensity of each ROI was also processed for each b-value separately (S_0, S_{500}, S_{1500}, S_{2500} for each ROI, with the subscripted numbers corresponding to the b-values).

Visual assessment. In the encephalopathy group, the DWI images at b = 1500 were assessed visually. Each ROI was assessed separately in terms of prominence (strength) and expanse of abnormal signal intensity, and was categorized into three groups:

severe, prominent abnormal signal intensity in more than 1/5 of the ROI; mild, prominent abnormal signal intensity between 1/10 and 1/5 of the ROI, or a slight abnormal signal intensity in more than 1/3 of the ROI; indistinct, prominence and expanse of abnormal signal intensity less than the above criteria (sample shown in Fig. 3). This categorization was first made by two board certified radiologists (Y.T. and T.O., 7-year and 20-year experience in MRI interpretation, respectively) independently. Both were blinded to any clinical information at the time of assessment. Finally, for ROIs for which categorizations differed between the interpreters, a final decision was reached by consensus.

Calculation of F_H and ADC. First, F_H was calculated for each ROI from the signal intensity of b = 500, 1500, and 2500 (S_{500}, S_{1500}, S_{2500}). The calculation method was the same as previously described in the "Calculation of F_H" section.

Second, ADCs were calculated for each ROI in four ways from the signal intensities of four different b-value pairs (S_0 and S_{1500}, S_0 and S_{500}, S_{500} and S_{1500}, and S_{1500} and S_{2500}), based on the assumption of monoexponential signal attenuation (ADC_{0-1500}, ADC_{0-500}, $ADC_{500-1500}$, and $ADC_{1500-2500}$; pairs of subscripted numbers are pairs of b-values used to calculate ADC). ADC_{0-1500}
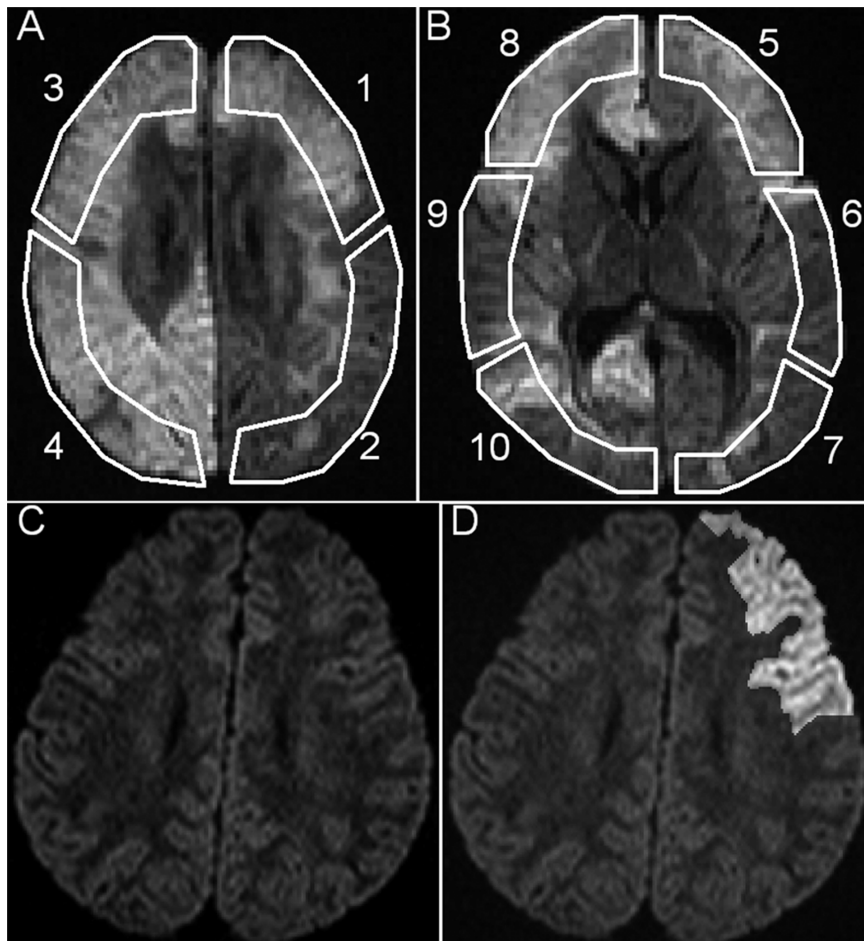

Figure 2. Regions of interest (ROIs) for the ROI-based study. A, B: Images acquired from a 1-year-old boy of unspecific acute encephalopathy. The images show the two specific slice levels selected for evaluation: the slice at the level of cerebral hemisphere (A), and the slice at the level of cerebral basal ganglia (B). Ten regions of interests (ROIs) were set as schematically illustrated for further assessments. C, D: A sample of accurate ROI 1 (frontal lobe of left cerebral hemisphere) acquired from a 2-year-old boy with suspected labium dyskinesia but which regressed a while after the examination (control group). C: Diffusion-weighted image before setting ROIs. D: Brightened area indicates the selected ROI, from which the pixels of cerebrospinal fluid and deep white matter were excluded as much as possible.
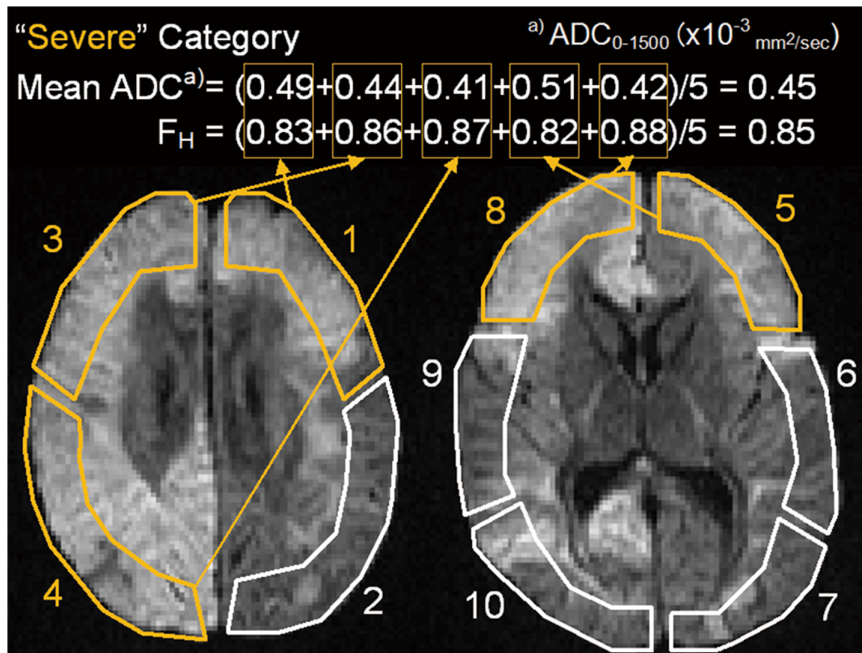doi:10.1371/journal.pone.0063869.g002

Figure 3. Mean F_H and ADC calculated in the encephalopathy group for analysis. Mean fraction of high b-pair (F_H) and apparent diffusion coefficient (ADC) for statistics were calculated for each patient. For the patients in the encephalopathy group, mean F_H and ADCs were calculated for each category separately by averaging F_H and ADCs across the regions of interests (ROIs) corresponding to each category. In this case (same case as in Fig. 2), five ROIs (ROIs 1, 3, 4, 5, and 8) corresponded to the "Severe" category, so the mean F_H and ADC (only ADC calculated by b-value = 0 and 1500 (ADC_{0-1500}) is shown here as example) for the "Severe" category was the averaged F_H and ADC of the five ROIs. In this case, ROIs 7, 9, and 10 were categorized as "mild" and ROIs 2 and 6 as "indistinct". Note: the schematic ROIs illustrated on the images seem to include deep white matter and cerebrospinal fluid, but the accurate ROIs for assessments did not include these areas (Fig. 2; D).
doi:10.1371/journal.pone.0063869.g003

was included to represent the most commonly used ADC in clinics. Third, to arrive at the final values for statistics, mean F_H and ADCs for each patient were calculated. In the control group, mean F_H and ADCs were calculated by averaging F_H and ADCs across all 10 ROIs. In the encephalopathy group, mean F_H and ADCs were calculated for each category separately by averaging F_H and ADCs across the ROIs corresponding to the category (Fig. 3).

Statistical analysis. In the control group, the relations between patient age and F_H and between patient age and ADC_{0-1500} were assessed using Spearman's rank correlation coefficient. Then, the mean F_H and ADCs calculated in the previous section for statistical purposes were compared between the control group and each category (severe, mild, and indistinct) of the encephalopathy group, respectively. Analysis of covariance (ANCOVA) was applied for these comparisons, with patient age being used as an additional variable. The P-values calculated by this procedure were tripled according to Bonferroni correction to avoid type 1 errors in the multiplicity of statistical analysis. A P-value (corrected in latter comparison) <0.05 was considered significant.

Results

Results of SNR Confirmation

The range and median of the ratio (i.e. mean signal intensity of b = 2500 divided by standard deviation of the signal intensity of b = 0) in the control group were: minimum, 4.36, maximum, 9.89, median, 6.35. The range and median of the ratio in the encephalopathy group were: minimum, 3.62, maximum, 9.04, median, 5.26. One patient in the encephalopathy group was

excluded from these results because abnormally high signal intensity was seen diffusely in the right caudate nucleus. Of note, the ratio of this patient was 15.9. The ratio was higher than 3.0 in all cases of both groups. The difference between the groups (the patient with abnormally high signal intensity in the right caudate nucleus was excluded) was not significant (Mann-Whitney test, P = 0.14).

Results of F_H Mapping

Some samples of F_H maps are shown in Fig. 4. The masking procedure worked well to abstract the approximate area of brain parenchyma. The map image was relatively noisy; however, the cortex and subcortical area of the patients in the encephalopathy group showed diffusely elevated F_H (color closer to red) compared to those in the control group (Fig. 4). The prominence of the elevation in F_H seemed to be related to the prominence of the abnormal signal intensity of DWI, but elevations of F_H were seen even in areas where there were no particular findings in DWI.

Results of ROI-based Study

The numbers of ROIs corresponding to each category of each patient of the encephalopathy group are shown in Table 2 (visual assessment). Of note, the categorization of 143 ROIs of 150 ROIs (10 ROIs each in 15 patients) was matched between the interpreters (95.3%), and the other 7 unmatched ROIs were decided by their consensus. The range and median of the number of ROIs categorized as "severe", "mild", and "indistinct" in each patient were 0–10 (4), 0–5 (1), and 0–10 (5), respectively (minimum–maximum, median in parentheses).

The correlation coefficient between F_H and patient age in the control group was 0.29, which was not significant (P = 0.28). The
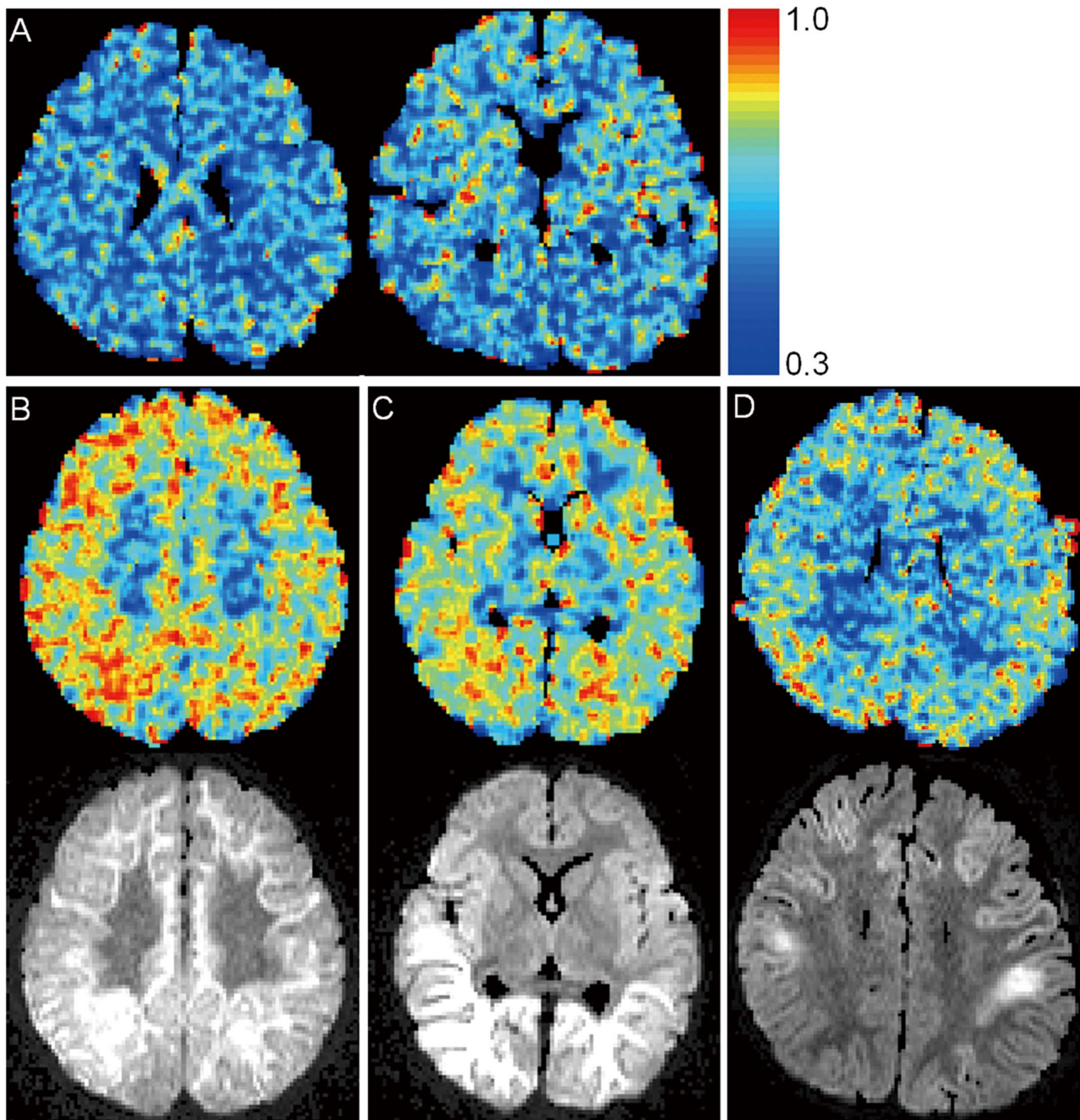
Figure 4. Samples of F_H map. A: F_H map (F_H: fraction of high b-pair) calculated from the images acquired from a 2-year-old boy in the control group (the same boy as in Fig. 2 C,D). B, C, and D: F_H maps (upper) and corresponding diffusion-weighted images (DWI) at b = 1500 (lower) of 1-year-old girl with unspecific encephalopathy (B), 1-year-old boy with acute encephalopathy with biphasic seizures and late reduced diffusion (AESD) (C), and another 1-year-old boy with AESD (D). F_H seems elevated in the cortical and subcortical areas of the encephalopathy group (B, C, and D) compared to the control group (A). The prominence of elevation in F_H seems related to the prominence of the abnormally high signal intensity in DWI, but the elevations of F_H are seen even in areas where there are no particular findings in DWI (e.g., posterior area of (D)).
doi:10.1371/journal.pone.0063869.g004

correlation coefficient between ADC_{0-1500} and patient age was −0.44, which indicated a negative tendency but without significance (P = 0.08). $ADC_{500-1500}$ was negatively correlated with age (r = −0.57) to a significant extent (P = 0.02). ADC_{0-500} and $ADC_{1500-2500}$ were not significantly correlated with patient age (P = 0.66 and 0.11, respectively).

Mean F_H in each category of the encephalopathy group (severe, mild, and indistinct) was higher than that of the control group, with all differences being statistically significant (P<0.05, corrected). On the other hand, mean ADC_{0-1500} was also lower in all three categories of the encephalopathy group compared to the control group, but significant differences were only found in the

Table 2. Categorization of ROIs of each patient in encephalopathy group.

Patient	age	sex	diagnosis	Number of ROIs		
				Severe	Mild	Indistinct
1	1	M	AESD	0	4	6
2	1	M	AESD	4	4	2
3	1	M	UC	5	3	2
4	1	F	ANE	10	0	0
5	10	F	UC	1	0	9
6	3	F	UC	3	5	2
7	2	M	UC	10	0	0
8	3	M	UC	1	2	7
9	1	F	AESD	1	1	8
10	1	M	UC	0	1	9
11	7	M	UC	0	0	10
12	1	F	UC	4	1	5
13	1	F	AESD	4	2	4
14	1	M	AESD	5	0	5
15	1	F	UC	10	0	0

ROIs: regions of interest, AESD: acute encephalopathy with biphasic seizures and late reduced diffusion, ANE: acute necrotizing encephalopathy, UC: uncategorizable.
doi:10.1371/journal.pone.0063869.t002

Table 3. Statistical analysis of F_H and ADC.

	Control	Encephalopathy		P-value [b]
F_H	0.735 (0.028)	Severe	0.810 (0.052)	<0.001
		Mild	0.773(0.033)	0.038
		Indistinct	0.765 (0.028)	0.015
ADC_{0-1500}[a]	0.879 (0.029)	Severe	0.645 (0.171)	<0.001
		Mild	0.838 (0.056)	0.027
		Indistinct	0.866 (0.050)	0.223
ADC_{0-500}[a]	1.097 (0.055)	Severe	0.804 (0.217)	<0.001
		Mild	1.021 (0.095)	0.111
		Indistinct	1.048 (0.069)	0.063
$ADC_{500-1500}$[a]	0.770 (0.029)	Severe	0.565 (0.150)	<0.001
		Mild	0.746 (0.047)	0.054
		Indistinct	0.774 (0.045)	1.477
$ADC_{1500-2500}$[a]	0.564 (0.040)	Severe	0.424 (0.120)	<0.001
		Mild	0.574 (0.045)	2.697
		Indistinct	0.595 (0.037)	0.533

Data denote the averages of the values, and standard deviations are in parentheses.
[a] $\times 10^{-3}$ mm^2/sec;
[b] Analysis of covariance between the control and encephalopathy groups (F_H, ADCs, and patient age as a variable); P-values were tripled according to the correction of Bonferroni. F_H: fraction of high b-pair, ADC: apparent diffusion coefficient; the pair of subscripted numbers indicate the pair of b-values used to calculate the value.
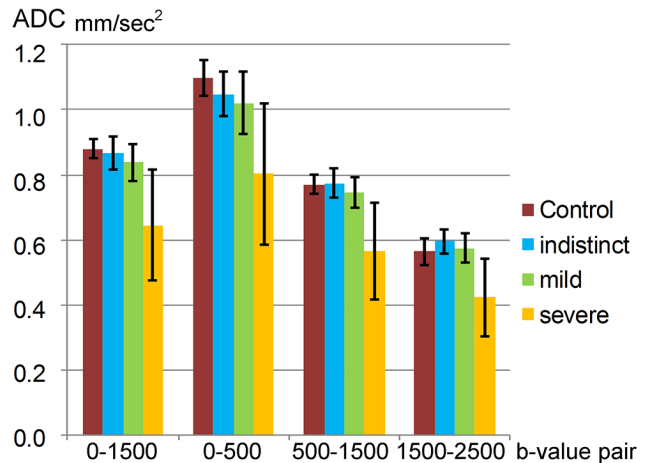doi:10.1371/journal.pone.0063869.t003

"severe" and "mild" categories. There was no significant difference between the "indistinct" category and the control group (P = 0.223, corrected) (Table 3).

Mean ADCs in the "severe" category were always lower than that of the control group with a significant difference regardless of the applied pair of b-values (b = 0 and 500, 500 and 1500, and 1500 and 2500); however, comparing the "indistinct" category and the control group, the mean ADC of the former tended to be lower (P = 0.063, corrected) in the low b-pair (b = 0, 500), but became even higher in the high b-pair (b = 1500, 2500), though the difference was not significant (Table 3, Fig. 5). Mean ADC of the "mild" category was between that of the "severe" and "indistinct" categories in each of the corresponding b-pairs. It was slightly higher than that of the control group in the high b-pair (b = 1500, 2500), but the difference was not significant (Table 3, Fig. 5).

Discussion

The SNR of the images obtained by the 4bDWI imaging sequence seems enough for the assessments even at b = 2500. In addition, difference between the control and encephalopathy groups was not significant. We evaluated the ratio of the mean signal intensity of b = 2500 and the standard deviation of the signal intensity of b = 0 instead of comparing the average signal intensity of b = 2500 directly with the background noise as usual. This was because it was difficult to evaluate the background noise accurately, since GRAPPA (a parallel imaging technique) was applied in the 4bDWI sequence. However, the ratio we assessed should be stricter than the "usual" SNR because the inhomogeneity of the caudate nucleus at b = 0 was also recognized as a noise in addition to the real noise in this method. Furthermore, the ROI was set near the center of the brain where the SNR is usually not good because of the distance from the coil. Thus the regions

Figure 5. ADCs of each category in each b-value pair. The bar graph shows the mean apparent diffusion coefficient (ADC) in each b-value pair in each category of the encephalopathy group. The error bar indicates standard deviations. The average ADC of the "indistinct" group was lower compared to the control group in the low b-pair (b = 0, 500), but it reversed toward the higher average in the high b-pair (b = 1500, 2500).
doi:10.1371/journal.pone.0063869.g005

assessed in this study (cortex and subcortical white matter) might have had higher SNRs. MR images in this study were acquired with either of two different coil sets depending on the patient's head size and age, but this we may not need consideration in this study because both obtained images with sufficient SNRs, and the differences between the groups were not significant.

The signal intensity of DWI was obtained only in four different b-values in this study, as the data were collected from the clinical database retrospectively. For this reason, it was inappropriate to fit the data directly to the biexponential equation (Introduction, Eq. 2). We calculated D_f, D_s, and f_s from S_0, S_{500}, S_{1500}, and S_{2500} by least-squares method (data not shown), but they had relatively large divergence, and agreements with those previously reported were poor [18–21,26]. In addition, the data failed to show a significant difference between the control and encephalopathy groups not only in the "indistinct" category but even in the "mild" category.

F_H in this study was designed as a value related to the two-compartment model of water diffusion in vivo that could be obtained from this small number of b-values. It was calculated by the theoretical signal intensity of b = 0 obtained from the signal intensity of the higher b-value pair (S_{1500}, S_{2500}) divided by the theoretical signal intensity of b = 0 calculated by the lower b-value pair (S_{500}, S_{1500}) (Fig. 1). The former value indicates the signal intensity at b = 0, in a theoretical case when there was only a "slower" diffusion component that could not have been totally attenuated by the b-value of 1500. On the other hand, the latter indicates the signal intensity at b = 0 when "faster" and "slower" diffusion components are both included. In addition, the effect of perfusion may not be included in this "slower" component because its signal might be attenuated at b = 500. Thus, F_H indicates the fraction of the "slower" diffusion component against the total diffusion except the very fast diffusion component including perfusion. This value seemed to have a positive correlation with f_s in the estimated range of D_s, D_f, and f_s in vivo (see Text S1). In addition, it also revealed a positive correlation with D_s, and a negative correlation with D_f at the same settings, a point that will be discussed later.

If there were more data points from a larger variation of the b-value, then D_f, D_s, and f_s could be more directly and accurately calculated by use of the least-squares method. However, more b-values would have required more scan time and more consistent sedation for juveniles. This was not suitable for clinical examination, especially for those with acute severe condition such as the acute encephalopathy discussed in this study. Thus, it stands to reason that, a simple method for assessing the two-compartment model should be the focus of discussion for applying this model in clinics; F_H was calculated from data that require only a clinically acceptable scan time, approximately 3 minutes, which in this regard might be a distinct advantage.

The correlation between $ADC_{500-1500}$ and patient age was significant in the control group, but the other values including F_H and ADC_{0-1500} (necessarily assessed in this study as a representative ADC used in clinics) showed no significant correlation between ages. However, considering the fact that patient age in the control and encephalopathy groups did not match (P = 0.01, Mann-Whitney test; details not shown), ANCOVA was applied for further statistical comparison to set patient age as an additional variable. Bonferroni correction was applied to avoid type 1 error.

The F_H map in this study (Fig. 4) revealed a diffusely increased F_H in the cortical and subcortical areas of the encephalopathy group patients. Furthermore, statistical comparison revealed that F_H achieved a significant difference between the control group and all three categories of the encephalopathy group (severe, mild, and indistinct). A probable mechanism for the difference may be a change in f_s. The exact mechanisms underlying the link between the diffusion parameters above (D_s, D_f, and f_s) and tissue microstructure remain largely unknown; however, one of the most accepted assumptions is that D_s and D_f provide intracellular and extracellular ADCs respectively, and thus f_s indicates the

fraction of intracellular volume [19]. Non-inflammatory brain edema and decrease in the size of extracellular space owing to cell (especially astrocyte) swelling have been pointed out in acute encephalopathy [29,30], which may in this respect increase f_s.

F_H demonstrated a significant difference between the control and encephalopathy groups even in the "indistinct" category, while ADC_{0-1500} (the ADC value usually used in clinics) did not show a significant difference in the same comparison. This result may indicate the higher detectability of F_H compared to ADC_{0-1500} regarding the less severe pathologic lesions of acute encephalopathy in the cortical and subcortical areas. However, our simulation (Text S1) showed that not only F_H but also ADC_{0-1500} reflects the change in f_s to some extent (Fig. S1; A, B in Text S1,). One mechanism that possibly contributed to the superiority of F_H compared to ADC_{0-1500} may be the increase of D_s in the slight change in acute encephalopathy (corresponding to the "indistinct" category). The increase in f_s and D_s synergistically increases F_H (both have a positive correlation with F_H, as described above) but works antagonistically in ADC_{0-1500}, and thus F_H has an advantage over ADC_{0-1500} in this setting (Fig. S1 in Text S1). The fact that ADCs of the "indistinct" category gradually become larger than the control group as the b-values enlarge (Table 3, Fig. 5) may at least slightly support this hypothesis. This is because D_s may be reflected more in the ADC of high b-pairs; the elevation of f_s may have a smaller effect in ADC of higher b-pairs, as the signal from the fast diffusion component is generally relatively attenuated by the motion proving gradient in high b-values, so that the importance of f_s might be limited, whereas the change in D_s might be greatly reflected in ADC of higher b-pairs. One possible mechanism for increasing D_s is the increased expression regulation of aquaporin-4 (AQP4). Recently, the relation of AQP4 regulation and brain edema was discussed in various pathologic states in mouse and human [31–34]. Up- or down-regulation of AQP4 seems quite complicated, so its mechanism is still not clear, although some of the aforementioned reports revealed an up-regulation of AQP in acute brain lesions [32,33]. Obata et al. discussed decreased D_s in the AQP knockout cell [35], which may contrarily indicate increased D_s in the up-regulated expression of AQP4. The relationship between pediatric acute encephalopathy and AQP4 is not yet well understood, so further studies will be required to confirm this hypothesis.

Another possible mechanism for the increase of D_s is the effect of a fever, which was more frequently seen in the encephalopathy group. It is well known that higher temperature induces more active molecular movement, which increases water diffusion. Recently, thermometry of CSF in the use of diffusion-weighted imaging has been well discussed [36–38]. Following the method discussed in the previous report [36], the diffusion coefficient of CSF in the lateral ventricle may increase by approximately 7% when body temperature increases from 36 to 38°C (2.9676 to 3.1102 mm/sec^2). Changes in D_s and D_f in hyperthermia have not been discussed, but it is conceivable that they may increase to some extent. Under such condition, $ADC_{1500-2500}$ may increase, as it reflects D_s.

In this respect, ADC_{0-1500}, ADC_{0-500}, and $ADC_{500-1500}$ should also have increased by the effect of increase in D_s, but the simultaneous increase in f_s (which is an increased fraction of a much slower diffusion (e.g. D_s) than D_f even if elevated as discussed), may have excessively worked antagonistically and thereby concealed this effect; $ADC_{1500-2500}$ might be less affected by the increased f_s, as it is related to D_s more directly than the other ADCs for the high b-values, so the effect from the change in the fraction of D_s (e.g. f_s) may be relatively limited.

Of note, it may be important that a febrile state may work anyway, antagonistically, for detecting diffusion restriction in the use of ADC, because the method is very commonly used in clinics regardless of this issue.

There was not enough data in this study to allow the evaluation of the detailed changes in D_s, and further study will be necessary. In addition, we may note that the ADC_{0-500} discussed above might be affected by perfusion. Another aspect of the result is that there may be some pathologic change in the encephalopathy group even in areas of unclear imaging findings. This suggests that acute encephalopathy is a pathologic condition of the whole brain, which well illustrates the discrepancy often experienced between the imaging findings and the clinical outcome – imaging findings do not always correspond exactly to the responsible area of impaired function. Recently, a mutation of the SCN1A gene (codes neuronal sodium channel alpha 1 subunit) was found to be the predisposing factor for the onset of various types of acute encephalopathy [14,17]. In addition, another report discussed genetic seizure susceptibility [16]. Pathologic mediation by cytokines has also been discussed in some cases of acute encephalopathy [2,39,40]. These non-focal factors may have caused diffuse alteration in water diffusion of the whole brain.

Our study has some limitations. It was a retrospective study with a relatively small sample size. In addition, selection was biased because 4bDWI was obtained only when the need was determined by an experienced radiologist, and excluding bias was difficult because all study imaging was performed as part of clinical care. Another limitation is that we discussed the encephalopathy cases altogether, regardless of their various clinical patterns that might have included different pathologies. However, as the pathologic mechanisms of acute encephalopathies are not well known, and approximately half of the cases in this study were non-specific, a more detailed grouping was difficult. Further studies with typical specific cases are necessary. In addition, further study and understanding of the pathogenesis of acute encephalopathies may be important. The last limitation is that the correlation between F_H and the two-compartment model, as well as the histological background to change in F_H, was not experimentally confirmed in this study. Further study may also be required concerning this point.

Conclusion

The results of the present study suggest that F_H is superior to ADC in detecting slight changes in cortical and subcortical white matter lesions in pediatric acute encephalopathy.

Supporting Information

Text S1 Appendix with fig. S1; Theoretical correlation between F_H, ADC and the two-compartment model.
(PDF)

Author Contributions

References

1. Hoshino A, Saitoh M, Oka A, Okumura A, Kubota M, et al. (2012) Epidemiology of acute encephalopathy in Japan, with emphasis on the association of viruses and syndromes. Brain Dev 34: 337–343.
2. Mizuguchi M, Yamanouchi H, Ichiyama T, Shiomi M (2007) Acute encephalopathy associated with influenza and other viral infections. Acta Neurol Scand Suppl 186: 45–56.
3. Morishima T, Togashi T, Yokota S, Okuno Y, Miyazaki C, et al. (2002) Encephalitis and encephalopathy associated with an influenza epidemic in Japan. Clin Infect Dis 35: 512–517.
4. Chen CI, Mar S, Brown S, Song SK, Benzinger TL (2011) Neuropathologic correlates for diffusion tensor imaging in postinfectious encephalopathy. Pediatr Neurol 44: 389–393.
5. Hayashi N, Okumura A, Kubota T, Tsuji T, Kidokoro H, et al. (2012) Prognostic factors in acute encephalopathy with reduced subcortical diffusion. Brain Dev 34: 632–639.
6. Kuwata S, Senzaki H, Urushibara Y, Toriyama M, Kobayashi S, et al. (2012) A case of acute encephalopathy with biphasic seizures and late reduced diffusion associated with Streptococcus pneumoniae meningoencephalitis. Brain Dev 34: 529–532.
7. Okumura A, Kidokoro H, Tsuji T, Suzuki M, Kubota T, et al. (2009) Differences of clinical manifestations according to the patterns of brain lesions in acute encephalopathy with reduced diffusion in the bilateral hemispheres. AJNR Am J Neuroradiol 30: 825–830.
8. Takanashi J, Oba H, Barkovich AJ, Tada H, Tanabe Y, et al. (2006) Diffusion MRI abnormalities after prolonged febrile seizures with encephalopathy. Neurology 66: 1304–1309; discussion 1291.
9. Shiihara T, Miyake T, Izumi S, Watanabe M, Kamayachi K, et al. (2012) Serum and cerebrospinal fluid S100B, neuron-specific enolase, and total tau protein in acute encephalopathy with biphasic seizures and late reduced diffusion: a diagnostic validity. Pediatr Int 54: 52–55.
10. Takanashi J (2009) Two newly proposed infectious encephalitis/encephalopathy syndromes. Brain Dev 31: 521–528.
11. Mizuguchi M (1997) Acute necrotizing encephalopathy of childhood: a novel form of acute encephalopathy prevalent in Japan and Taiwan. Brain Dev 19: 81–92.
12. Wong AM, Simon EM, Zimmerman RA, Wang HS, Toh CH, et al. (2006) Acute necrotizing encephalopathy of childhood: correlation of MR findings and clinical outcome. AJNR Am J Neuroradiol 27: 1919–1923.
13. Shinohara M, Saitoh M, Takanashi J, Yamanouchi H, Kubota M, et al. (2011) Carnitine palmitoyl transferase II polymorphism is associated with multiple syndromes of acute encephalopathy with various infectious diseases. Brain Dev 33: 512–517.
14. Okumura A, Uematsu M, Imataka G, Tanaka M, Okanishi T, et al. (2012) Acute encephalopathy in children with Dravet syndrome. Epilepsia 53: 79–86.
15. Tadokoro R, Okumura A, Nakazawa T, Hara S, Yamakawa Y, et al. (2010) Acute encephalopathy with biphasic seizures and late reduced diffusion associated with hemophagocytic syndrome. Brain Dev 32: 477–481.
16. Kobayashi K, Ouchida M, Okumura A, Maegaki Y, Nishiyama I, et al. (2010) Genetic seizure susceptibility underlying acute encephalopathies in childhood. Epilepsy Res 91: 143–152.
17. Saitoh M, Shinohara M, Hoshino H, Kubota M, Amemiya K, et al. (2012) Mutations of the SCN1A gene in acute encephalopathy. Epilepsia 53: 558–564.
18. Brugieres P, Thomas P, Maraval A, Hosseini H, Combes C, et al. (2004) Water diffusion compartmentation at high b values in ischemic human brain. AJNR Am J Neuroradiol 25: 692–698.
19. Clark CA, Le Bihan D (2000) Water diffusion compartmentation and anisotropy at high b values in the human brain. Magn Reson Med 44: 852–859.
20. Maier SE, Bogner P, Bajzik G, Mamata H, Mamata Y, et al. (2001) Normal brain and brain tumor: multicomponent apparent diffusion coefficient line scan imaging. Radiology 219: 842–849.
21. Maier SE, Mulkern RV (2008) Biexponential analysis of diffusion-related signal decay in normal human cortical and deep gray matter. Magn Reson Imaging 26: 897–904.
22. Schwarcz A, Bogner P, Meric P, Correze JL, Berente Z, et al. (2004) The existence of biexponential signal decay in magnetic resonance diffusion-weighted imaging appears to be independent of compartmentalization. Magn Reson Med 51: 278–285.
23. Shinmoto H, Oshio K, Tanimoto A, Higuchi N, Okuda S, et al. (2009) Biexponential apparent diffusion coefficients in prostate cancer. Magn Reson Imaging 27: 355–359.
24. Tamura T, Usui S, Murakami S, Arihiro K, Akiyama Y, et al. (2010) Biexponential Signal Attenuation Analysis of Diffusion-weighted Imaging of Breast. Magn Reson Med Sci 9: 195–207.
25. Tamura T, Usui S, Murakami S, Arihiro K, Fujimoto T, et al. (2012) Comparisons of multi b-value DWI signal analysis with pathological specimen of breast cancer. Magn Reson Med 68: 890–897.
26. Mulkern RV, Gudbjartsson H, Westin CF, Zengingonul HP, Gartner W, et al. (1999) Multi-component apparent diffusion coefficients in human brain. NMR Biomed 12: 51–62.
27. Lee JH, Springer CS Jr (2003) Effects of equilibrium exchange on diffusion-weighted NMR signals: the diffusigraphic "shutter-speed". Magn Reson Med 49: 450–458.
28. Mardor Y, Pfeffer R, Spiegelmann R, Roth Y, Maier SE, et al. (2003) Early detection of response to radiation therapy in patients with brain malignancies

using conventional and high b-value diffusion-weighted magnetic resonance imaging. J Clin Oncol 21: 1094–1100.

29. Takanashi J, Tada H, Terada H, Barkovich AJ (2009) Excitotoxicity in acute encephalopathy with biphasic seizures and late reduced diffusion. AJNR Am J Neuroradiol 30: 132–135.

30. Traul DE, Traul CS, Matsumoto J, Goodkin HP (2008) Acute encephalopathy with biphasic seizures and late restricted diffusion on MRI in a Japanese child living in the USA. Dev Med Child Neurol 50: 717–719.

31. Benga O, Huber VJ (2012) Brain water channel proteins in health and disease. Mol Aspects Med 33: 562–578.

32. Ribeiro Mde C, Hirt L, Bogousslavsky J, Regli L, Badaut J (2006) Time course of aquaporin expression after transient focal cerebral ischemia in mice. J Neurosci Res 83: 1231–1240.

33. Badaut J, Lasbennes F, Magistretti PJ, Regli L (2002) Aquaporins in brain: distribution, physiology, and pathophysiology. J Cereb Blood Flow Metab 22: 367–378.

34. Matsushita T, Isobe N, Matsuoka T, Ishizu T, Kawano Y, et al. (2009) Extensive vasogenic edema of anti-aquaporin-4 antibody-related brain lesions. Mult Scler 15: 1113–1117.

35. Obata T, Kershaw J, Kuroiwa D, Shibata S, Abe Y, et al. (2012) Effect of Cell Membrane Water Permeability on Diffusion-Weighted MR Signal: A Study Using Expression-Controlled Aquaporin4 Cells. 20th Annual Meeting, International Society for Magnetic Resonance in Medicine, Melbourne: 1830.

36. Sakai K, Yamada K, Sugimoto N (2012) Calculation methods for ventricular diffusion-weighted imaging thermometry: phantom and volunteer studies. NMR Biomed 25: 340–346.

37. Sakai K, Yamada K, Mori S, Sugimoto N, Nishimura T (2011) Age-dependent brain temperature decline assessed by diffusion-weighted imaging thermometry. NMR Biomed 24: 1063–1067.

38. Kozak LR, Bango M, Szabo M, Rudas G, Vidnyanszky Z, et al. (2010) Using diffusion MRI for measuring the temperature of cerebrospinal fluid within the lateral ventricles. Acta Paediatr 99: 237–243.

39. Ichiyama T, Ito Y, Kubota M, Yamazaki T, Nakamura K, et al. (2009) Serum and cerebrospinal fluid levels of cytokines in acute encephalopathy associated with human herpesvirus-6 infection. Brain Dev 31: 731–738.

40. Ichiyama T, Suenaga N, Kajimoto M, Tohyama J, Isumi H, et al. (2008) Serum and CSF levels of cytokines in acute encephalopathy following prolonged febrile seizures. Brain Dev 30: 47–52.

10